Korean J. Chem. Eng., 37(6), 961-968 (2020)
DOI: 10.1007/s11814-020-0525-2

pISSN: 0256-1115
eISSN: 1975-7220

Kinetics and mechanism study of H-acid degradation by peroxymonosulfate activation with Co_3O_4-Fe_2O_3/Al_2O_3

Ping Dai*, Xiaowei Sun, Dongyan Xu**,†, and Feng Tan*****

*College of Electromechanical Engineering, Qingdao University of Science & Technology, Qingdao, P. R. China
**College of Chemical Engineering, Qingdao University of Science & Technology, Qingdao, P. R. China
***Key Laboratory of Industrial Ecology and Environmental Engineering (Ministry of Education), School of Environmental Science and Technology, Dalian University of Technology, Dalian, P. R. China
(*Received 26 December 2019 • accepted 27 February 2020*)

Abstract−Alumina supported bimetallic cobalt-iron oxide (Co_3O_4-Fe_2O_3/Al_2O_3) catalyst was prepared via co-impregnation of boehmite with the mixture solution of cobalt nitrate and iron nitrate followed by calcination in air. X-ray photoelectron spectroscopy and high-resolution transmission electron microscope analyses confirmed the existence of highly dispersed Co_3O_4 and Fe_2O_3 nanoparticles in the as-prepared catalysts. The catalytic activity of Co_3O_4-Fe_2O_3/Al_2O_3 was evaluated for the degradation of H-acid in aqueous solution by heterogeneous activation of peroxymonosulfate. The results indicated that the Co_3O_4-Fe_2O_3/Al_2O_3 catalyst exhibited an identical initial activity but much better recyclability than Co_3O_4/Al_2O_3 due to its low amount of metal leaching and possible redox circle of Co(II)/Co(III). Electron paramagnetic resonance spectroscopy and radical quenching experiments suggested that singlet oxygen ($^1O_2$) contributed much more than ·OH and $SO_4^{\bullet-}$ to H-acid degradation, and the degradation mainly followed a nonradical reaction mechanism.

Keywords: H-acid, Peroxymonosulfate, Degradation, Singlet Oxygen, Cobalt, Iron

INTRODUCTION

H-acid, 1-amino-8-naphthol-3,6-disulfonic acid, is an important intermediate in the synthesis of acid, reactive, azo, and direct dyes. The extensive use of H-acid has inevitably resulted in its release to wastewaters that are detrimental to human health and ecosystem [1,2]. The highly soluble nature of H-acid makes it more difficult to treat H-acid-containing wastewater by conventional physical, chemical, and biological methods [3]. Therefore, it is of great significance to search for efficient methods that can realize complete degradation of H-acid in the wastewaters.

Advanced oxidation processes (AOPs) based on in situ generation of hydroxyl radical (·OH) by activation of H_2O_2 with Fe^{2+} have been demonstrated as efficient methods to degrade target aqueous pollutants [4,5]. However, the Fenton reaction and its modifications still suffer from several drawbacks, such as safety associated with transport and storage of H_2O_2, pH dependence of the reaction, large amount of sludge produced, and slow kinetics of ferrous iron regeneration [6]. Compared with hydroxyl radical (·OH, 1.8-2.7 eV), sulfate radical possesses higher redox potential (2.5-3.1 eV) at neutral pH and longer half-life and is more selective for the oxidation of organic compounds [7]. Generally, $SO_4^{\bullet-}$ can be generated by homogeneous activation of persulfate (PS, $S_2O_8^{2-}$) or peroxymonosulfate (PMS, HSO_5^-) with various transition metals, of which Co^{2+} exhibits the highest activity towards PMS activation and thus achieves outstanding decontamination of organic pollutants [8].

Although the homogeneous activation of PMS can avoid the involvement of high-energy inputs, the recovery of homogenous catalysts is very difficult. Particularly, the massive usage of cobalt ions may cause additional contamination problems due to their toxicity, making the homogeneous Co^{2+}/PMS system being not technically or economically feasible. To date, various alternative heterogeneous catalysts including bulk cobalt oxides [9,10] and supported cobalt catalysts [11-13] have been widely investigated for the purpose of catalyst recycling and repetitive usage. Additionally, many efforts have been devoted to improving the performance or solving the leaching problem of monometallic cobalt catalysts by substituting a part of cobalt ions with other metals [14,15]. Although iron is not as effective as cobalt for activating PMS, its conjugation with PMS is still attractive because of iron's low toxicity to the environment [16]. Alumina supported iron catalysts, which have been successfully applied to various Fenton-like processes, display enhanced performance for the catalytic wet peroxide oxidation of different organic pollutants owing to the amphoteric nature and good adsorption ability of alumina as well as the advantageous Fe-Al interactions [17]. More importantly, the strong metal-metal interactions could help inhibit the cobalt leaching from the bimetallic Fe-Co catalysts [18]. Therefore, simultaneously anchoring Fe and Co on alumina is anticipated to improve the stability of the catalysts. However, little effort has been made to try to overcome the drawbacks of monometallic catalysts as an activator of PMS by incorporating cobalt and iron oxides into alumina support and further to investigate the mechanism of PMS activation on the as-prepared catalyst.

Herein, alumina supported bimetallic cobalt-iron catalyst was

†To whom correspondence should be addressed.
E-mail: xdy0156@qust.edu.cn
Copyright by The Korean Institute of Chemical Engineers.

prepared and used to activate PMS for the degradation of H-acid in aqueous solution. The catalytic degradation kinetics of H-acid was systematically investigated. Moreover, radical quenching tests and electron paramagnetic resonance (EPR) studies were performed to elucidate the mechanism of PMS activation over Co_3O_4-Fe_2O_3/Al_2O_3 for the first time.

MATERIALS AND METHODS

1. Materials and Chemicals

Boehmite (250 $m^2 \cdot g^{-1}$) was purchased from Shandong Alumina Plant, China. Commercial grade H-acid (8-Amino-1-naphthol-3,6-disulfonic acid monosodium salt), iron (III) nitrate nonahydrate and cobalt (II) nitrate hexahydrate were obtained from Sinopharm Chemical Reagent Co., Ltd., China. The potassium monopersulfate triple salt (PMS, $KHSO_5 \geq 47\%$), 5,5-Dimethyl-1-pyrroline-N-oxide (DMPO, 97%), 2,2,6,6-Tetramethylpiperidone (TEMP, 98%), *L*-histidine, and *p*-benzoquinone (*p*-BQ) were purchased from Shanghai Aladdin Bio-Chem Technology Co., Ltd.

2. Catalyst Preparation

The alumina supported bimetallic cobalt-iron catalyst was prepared by means of one-step incipient wetness impregnation of boehmite using aqueous solution of cobalt nitrate and iron nitrate. In a typical preparation procedure, the 5 wt% Co_3O_4-Fe_2O_3/Al_2O_3 catalyst with a Co/Fe mass ratio of 2.0 was prepared by impregnation of boehmite (5 g) with an aqueous mixture solution containing cobalt nitrate (0.8803 g) and iron nitrate (0.6110 g). The impregnated boehmite was then dried at 383 K for 12 h and calcined at 550 °C for 5 h in air. The samples with different metal loadings ranging from 1 to 10 wt% were obtained by controlling the concentrations of cobalt and iron ions in the mixture solution. For comparison, 5 wt% Co_3O_4/Al_2O_3 was also prepared by using the same method.

3. Catalyst Characterization

Powder X-ray diffraction (XRD) patterns of support and catalysts were recorded on a D/max-2500/PC X-ray diffractometer (Rigaku, Japan) with a Cu Kα radiation source at 40 kV and 150 mA. Field emission scanning electron microscopy (JEOL JSM 6700F) and transmission electron microscopy (JEM-2010F, JEOL) with a field emission gun of 200 kV were employed to investigate the morphology of the samples. The elemental valence states were investigated by X-ray photoelectron spectroscopy (ESCALAB 250XI, Thermo Fisher Scientific, USA) equipped with a monochromatic Al Kα X-ray source at a pass energy of 30 eV. The C1s peak at 284.6 eV was used to calibrate peak positions. The levels of metal leaching were determined by inductively coupled plasma mass (ICP-MS) spectrometry (Agilent 7700, USA).

4. Degradation Experiments

The catalytic degradation experiments were carried out in a 100 mL glass bottle installed in a constant temperature water bath. Before the degradation reaction, a proper amount of catalyst and 50 mL H-acid aqueous solution were added into the reactor, and then the solution was magnetically stirred for 30 min to achieve adsorption-desorption equilibrium. The reaction was initiated by adding appropriate amount of PMS into the reactor. For a typical test, the concentrations of H-acid, PMS and catalysts were 20 mg/L, 1.2 mM and 0.5 g/L, respectively. At predetermined time intervals during degradation, a 4 mL sample was withdrawn from the suspension, and then 0.2 ml methanol was quickly injected to the sample to prevent further reaction. After removing the catalyst by filtration with a 0.45 μm film, the residual concentration of H-acid was determined by using a UV-vis spectrophotometer (Yoke). For the quenching experiments, a known amount of quench reagent, such as methanol (MeOH), tert-butanol (TBA), *L*-histidine, and *p*-benzoquinone (*p*-BQ), was added into the RhB solution before the addition of PMS.

5. Mechanistic Studies

To verify the active species generated in the Co_3O_4-Fe_2O_3/Al_2O_3/PMS/H-acid system, EPR experiments were conducted with an electron paramagnetic resonance spectrometer (Bruker A200, Germany) using DMPO and TEMP as the spin-trapping agents to detect $\cdot OH/SO_4^{\cdot-}$ and $^1O_2$, respectively. For comparison, EPR experiments on PMS alone and Co_3O_4-Fe_2O_3/Al_2O_3/PMS systems were also conducted. Typically, 1 mL sample was withdrawn from Co_3O_4-Fe_2O_3/Al_2O_3/PMS/H-acid system (H-acid concentration: 20 mg/L, catalyst dosage: 0.5 g/L, and PMS: 0.6 mM) and then mixed with 40 μL DMPO or TEMP solution. A quartz capillary tube was used to suck up the mixed solution to detect corresponding signals from spin-trapping adducts in the EPR.

RESULTS AND DISCUSSION

1. Characterization of Co_3O_4-Fe_2O_3/Al_2O_3

The XRD patterns of boehmite and the Co_3O_4-Fe_2O_3/Al_2O_3 catalysts with different metal loadings are shown in Fig. 1. The as-received boehmite exhibited typical (020), (120), (031), and (051) planes of AlOOH (JCPDS, 49-0133). For the Co_3O_4-Fe_2O_3/Al_2O_3-group catalysts, the diffraction peaks centered at 37.5, 45.7 and 67.0° were indexed to γ-Al_2O_3 (JCPDS, 10-0425) with low crystallinity, suggesting the transformation of boehmite to γ-Al_2O_3 during the calcination process. No metallic oxide phases could be detected for the 1 wt% and 2 wt% Co_3O_4-Fe_2O_3/Al_2O_3 catalysts owing to the low metal content and/or high metal dispersion. However, some

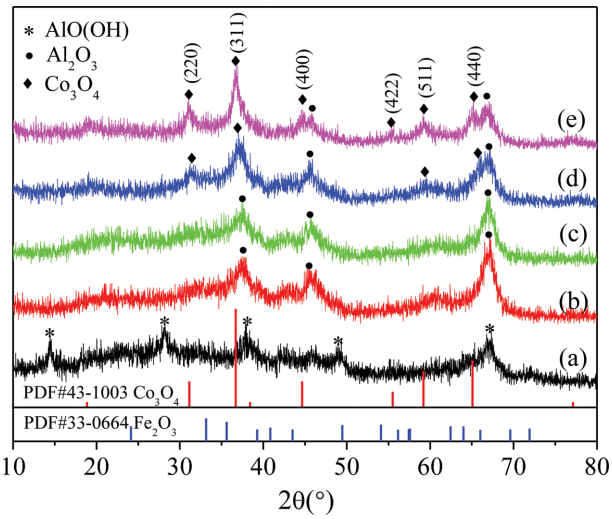


Fig. 1. XRD patterns of boehmite (a), 1 wt% (b), 2 wt% (c), 5 wt% (d), and 10 wt% (e) Co_3O_4-Fe_2O_3/Al_2O_3.

broad and weak reflexes centered at 2θ=31.2, 36.8, 44.7, 55.4, 59.2, and 65.2° ascribed to Co_3O_4 (JCPDS, 43-1003) crystallites were observed when the metal content amounts to 5 wt%. Note that Fe_2O_3 phase was still undetectable on account of low content.

The representative morphologies of 5 wt% Co_3O_4-Fe_2O_3/Al_2O_3 catalyst are displayed in Fig. 2. The SEM micrograph shows the presence of irregular Al_2O_3 clusters formed by the agglomeration of nanocrystallites (Fig. 2(a)). As displayed in Fig. 2(b), the Co_3O_4-

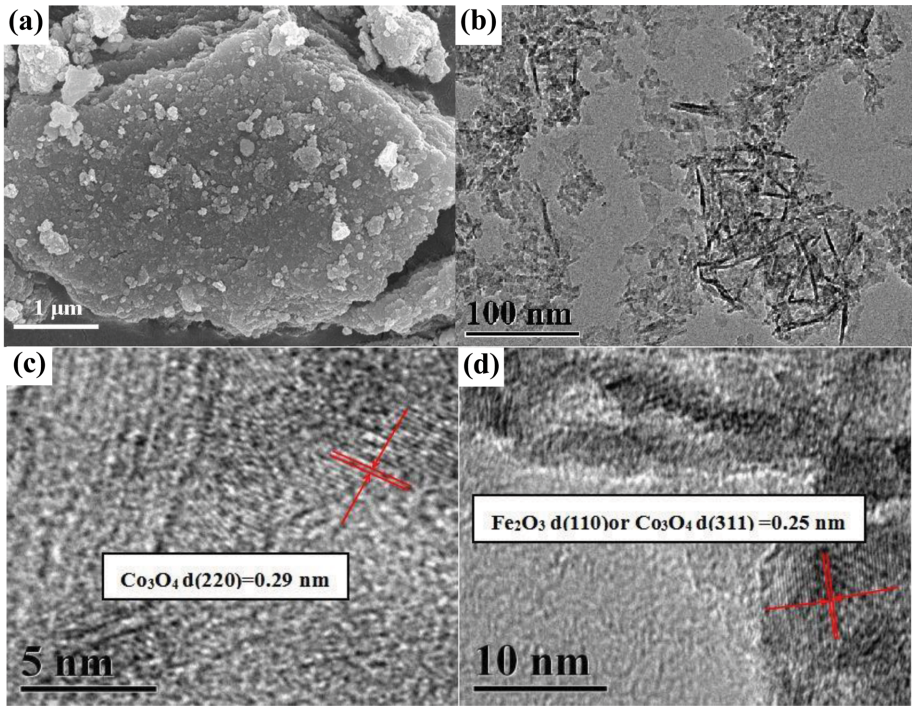


Fig. 2. SEM (a), TEM (b) and HR-TEM (c), (d) images of 5 wt% Co_3O_4-Fe_2O_3/Al_2O_3.

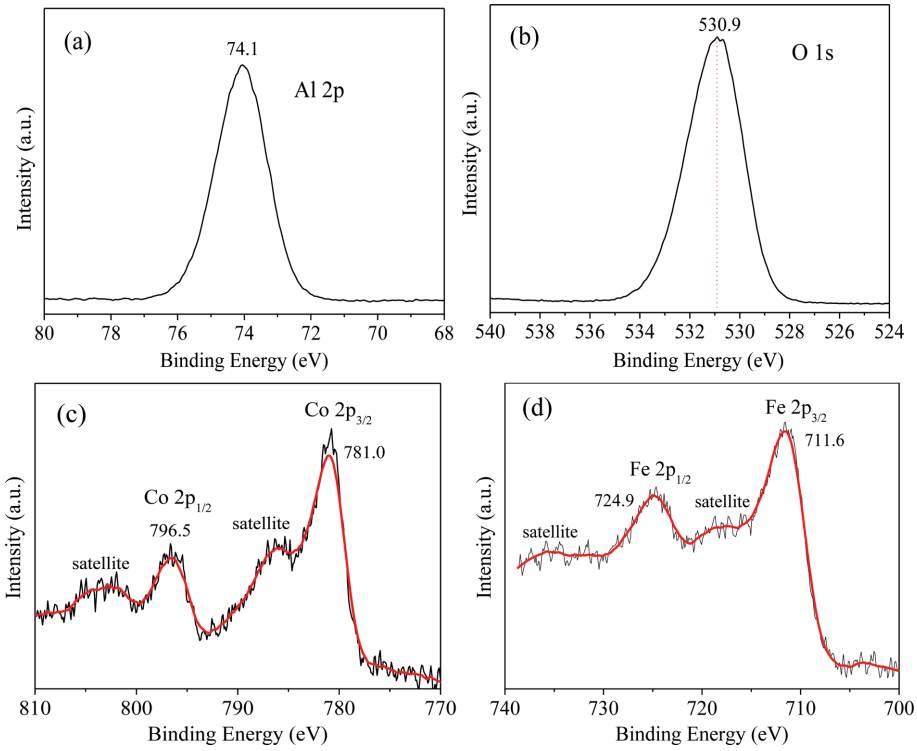


Fig. 3. XPS spectra of O 1s (a), Al 2p (b), Co 2p (c), and Fe 2p (d) for 5 wt% Co_3O_4-Fe_2O_3/Al_2O_3.

Fe_2O_3/Al_2O_3 catalyst displays rather similar microstructure as γ-Al_2O_3 in which interconnected rod-like particles make up the three-dimensional porous structure [19,20]. No large Co_3O_4 and Fe_2O_3 agglomerates can be observed because of better metal dispersion. The *d*-spacing of 0.29 nm corresponded to (220) plane of cubic Co_3O_4 (Fig. 2(c)) [21]. The *d*-spacing of 0.25 nm is in good agreement with the (110) plane of cubic Co_3O_4 or (311) plane of Fe_2O_3 (Fig. 2(d)) [22,23].

High-resolution Co 2p, Fe 2p, C 1s, and O 1s XPS spectra of 5 wt% Co_3O_4-Fe_2O_3/Al_2O_3 were analyzed to further verify the presence of Co_3O_4 and Fe_2O_3. A major Al 2p peak centered at around 74 eV agrees well with the oxidized Al in Al_2O_3 (Fig. 3(a)). The major peak of O 1s centered at around 530.9 eV was assigned to the lattice oxygen bonded with Co^{2+}, Co^{3+} and Fe^{3+} [24,25]. Fig. 3(c) shows the XPS spectrum of Co 2p of the Co_3O_4-Fe_2O_3/Al_2O_3 sample. The main peaks centred at 781.0 eV and 796.5 eV match with Co $2p_{3/2}$ and Co $2p_{1/2}$, respectively. In addition, two shakeup satellites with low intensity are present at approximately 6 eV above the main peaks and indexed to Co_3O_4. Particularly, the band gap of 15.5 eV between Co $2p_{3/2}$ and Co $2p_{1/2}$ indicates the existence of Co^{2+} and Co^{3+} [26]. Likewise, the Co_3O_4-Fe_2O_3/Al_2O_3 sample exhibits Fe $2p_{3/2}$ and Fe $2p_{1/2}$ peaks as well as their weak satellite peaks (Fig. 3(d)). The Fe $2p_{3/2}$ and Fe $2p_{1/2}$ peaks appear at approximately 711.6 and 724.9 eV, respectively, which is consistent with characteristic Fe^{3+} ions [27,28].

2. Catalytic Activity

Fig. 4(a) shows the catalytic performance of the Co_3O_4-Fe_2O_3/Al_2O_3-group catalysts for H-acid degradation in the presence of PMS. Obviously, the catalytic activity was significantly dependent on the metal loading of Co_3O_4-Fe_2O_3/Al_2O_3. The degradation effi-

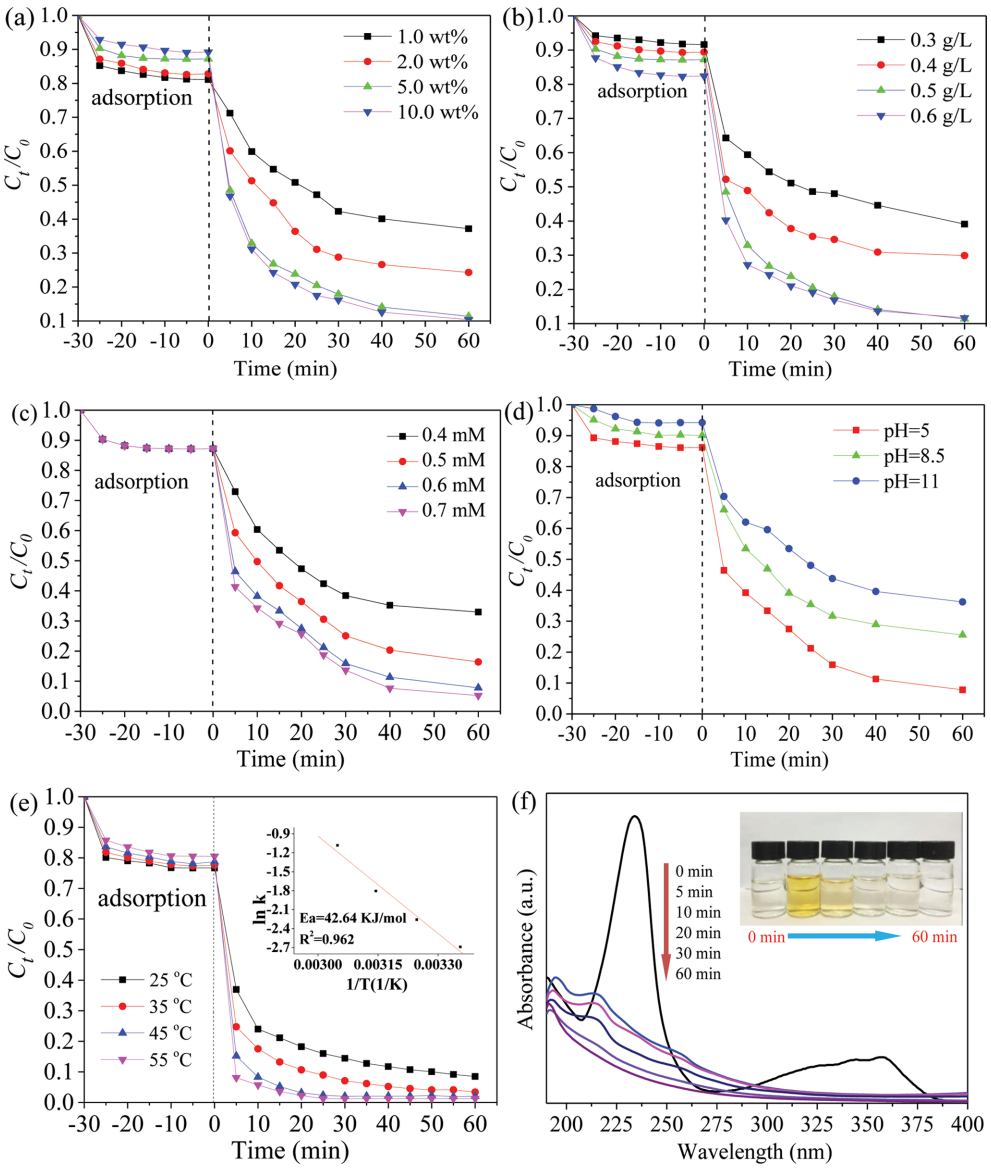


Fig. 4. Effects of metal content (a), catalyst dosage (b), PMS concentration (c), pH (d) and reaction temperature (e) on H-acid degradation; Temporal UV-vis absorption spectral changes during the degradation of H-acid (f). Reaction conditions: $[H\text{-acid}]_0$=20 mg/L, $[PMS]_0$= 0.6 mM, pH=5.0, T=25 °C, [catalyst]=0.5 g/L.

ciency of H-acid was markedly improved by increasing the metal loading from 1.0 to 5.0 wt%, which is due to the increment of active sites available. However, when the metal loading was further increased to 10.0 wt%, the degradation efficiency of H-acid changed little, possibly owing to the agglomeration of metal oxides and pore blockage. As expected, the adsorption and degradation of H-acid also showed a positive dependence on Co_3O_4-Fe_2O_3/Al_2O_3 dosage (Fig. 4(b)). The efficiency increased continuously as Co_3O_4-Fe_2O_3/Al_2O_3 dosage was increased from 0.3 to 0.5 g/L at fixed PMS dose, which could be attributed to the increased amount of active sites for activation of PMS to generate more ROSs within the same reaction time. Further increasing the dosage to 0.6 g/L, the degradation efficiency leveled off. The degradation efficiency of H-acid can be largely improved by increasing the concentration of PMS (Fig. 4(c)). When the concentration of PMS was increased from 0.4 to 0.6 mmol/L, the degradation efficiency increased from 67.1% to 92.2%. Further increasing the concentration from 0.6 to 0.7 mmol/L resulted in a slight increase in degradation efficiency. The H-acid degradation experiments were also carried out at different pH of 5, 8.5 and 11 (Fig. 4(d)). It is obvious that the degradation efficiency in acidic condition was higher than that in neutral and alkaline conditions because strong alkaline condition could induce PMS to deprotonate and transform into less oxidative SO_5^{2-}, leading to the decrease of degradation efficiency [29]. In addition, the solution pH was reduced after reaction due to the formation of acid intermediates (not shown).

The influence of reaction temperature on H-acid degradation is presented in Fig. 4(e). The elevated reaction temperature caused substantially enhanced effects on both PMS activation and degradation kinetics, and thus improved the degradation efficiency. The rate constants (k) were obtained based on pseudo-first-order kinetics, and the activation energy was calculated to be 42.6 kJ/mol through the plot of 1/T vs. ln k from inset of Fig. 4(e).

The variation in H-acid degradation with time for the Co_3O_4-Fe_2O_3/Al_2O_3/PMS system was monitored by collecting UV-visible spectra (Fig. 4(f)). H-acid displays two UV absorption bands centered at 358 and 234 nm. The strong absorption at low wavelength is the characteristic naphthalene structure of H-acid. It was found that the main absorption bands disappeared and two new bands appeared at 195 and 215 nm after 5 min of reaction, which indicated that the naphthalene ring was destroyed and other intermediate compounds formed during reaction [30]. These intermediate bands gradually declined and diminished after 60 min of reaction. The degradation process was also accompanied by the color change of the reactant solution. It was observed that the reaction solution was deepened firstly, which was ascribed to oxidation of the -NH_2 chromophore in the H-acid molecule into -NO_2 [31]. Then the color of the solution turned light steadily with the ring open of nitro-aromatic hydrocarbon.

3. Reusability

The reusability is vital for the practical application of heterogeneous catalysts. The reusability of Co_3O_4/Al_2O_3 and Co_3O_4-Fe_2O_3/Al_2O_3 was investigated by repetitive degradation reactions over the recycled catalysts (Fig. 5). The degradation efficiency decreased from 94.1% to 70.3% and form 92.2% to 84.2% afer four successive runs for Co_3O_4/Al_2O_3 and Co_3O_4-Fe_2O_3/Al_2O_3, respectively,

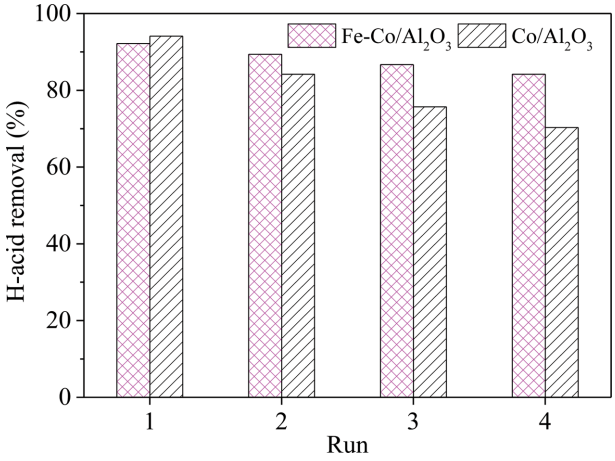


Fig. 5. Reusability of the 5 wt% Co_3O_4-Fe_2O_3/Al_2O_3 catalyst for H-acid degradation. Reaction conditions: $[H\text{-acid}]_0$=20 mg/L, $[PMS]_0$=0.6 mM, [catalyst]=0.5 g/L, pH=5.0, T=25 °C.

indicating that the Co_3O_4-Fe_2O_3/Al_2O_3 catalyst possessed superior reusability to the Co_3O_4/Al_2O_3 catalyst. The levels of metal leaching were verified to be 77.5 μg/L and 38.2 μg/L for Co_3O_4/Al_2O_3 and Co_3O_4-Fe_2O_3/Al_2O_3, respectively. In addition to the inevitable metal leaching, the poisoning of active sites by adsorption of degradation intermediates may cause activity deterioration [32]. Previous studies also demonstrated that the rate-limiting process for PMS activation is the generation of Co^{2+}-OH complexes derived from H_2O dissociation with Co^{2+} and that Co_3O_4 is inferior in this process since the Co^{2+}-OH complexes are hardly regenerated once they are consumed [16,33]. It was suggested that the existence of Fe^{3+} can help the regeneration of Co^{2+}-OH complexes via the redox cycles of metals ($M^{2+}\leftrightarrow M^{3+}\leftrightarrow M^{2+}$) during the PMS oxidation [26]. Similarly, the co-incorporation of Co and Cu bimetallic oxides in CuCo@ZnO leads to a higher surface hydroxyl density [34,35]. Therfore, it can be deduced that simultaneously anchoring Fe and Co on alumina is beneficial to altering the redox circle of Co(II)/Co(III) and thus improving the activation of PMS.

4. Identification of the Reactive Species

A series of radical-quenching experiments were carried out to identify the ROSs that could be possibly generated by activating PMS with Co_3O_4-Fe_2O_3/Al_2O_3 and evaluate their contributions to H-acid degradation (Fig. 6). Herein, methanol, *tert*-butanol, *L*-histidine and *p*-benzoquinone were used as the scavengers for $SO_4^{-\bullet}$, ·OH, singlet oxygen ($^1O_2$) and superoxide anion radical ($O_2^{-\bullet}$), respectively. Upon the addition of excess *tert*-butanol and methanol, the degradation of H-acid within 60 min decreased from 88.8% to 80.6% and 73.4%, respectively. These results indicate that both ·OH and $SO_4^{-\bullet}$ were definitely produced but neither of them was the main contributor to H-acid degradation. Similar results were also reported for selective degradation of sulfonamide antibiotics by PMS alone [36], paracetamol removal in the Fe-N@C/PMS system [37], and oxidative degradation of persistent contaminants in the N-doped graphene/PMS system [38]. Furthermore, an excessive introduction of *p*-benzoquinone exhibited very limited inhibition effect on H-acid degradation, suggesting that involvement of $O_2^{-\bullet}$ in the degradation of H-acid could be reasonably ruled out. In compari-

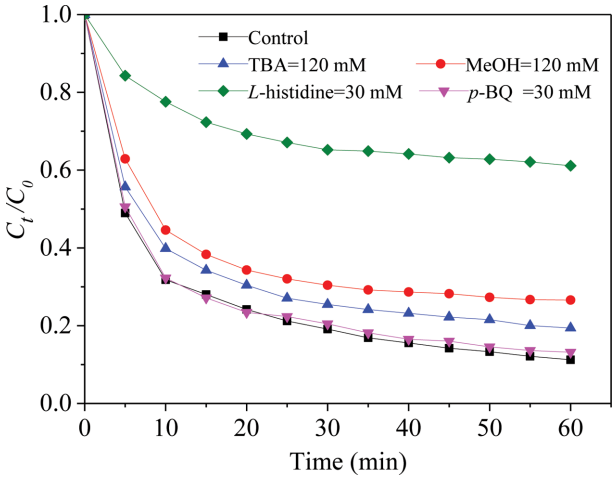


Fig. 6. Effect of different radical quenchers on H-acid degradation in Co_3O_4-Fe_2O_3/Al_2O_3/PMS system. Reaction conditions: [H-acid]$_0$=20 mg/L, [PMS]$_0$=0.6 mM, [catalyst]=0.5 g/L, pH=5.0, T=25 °C.

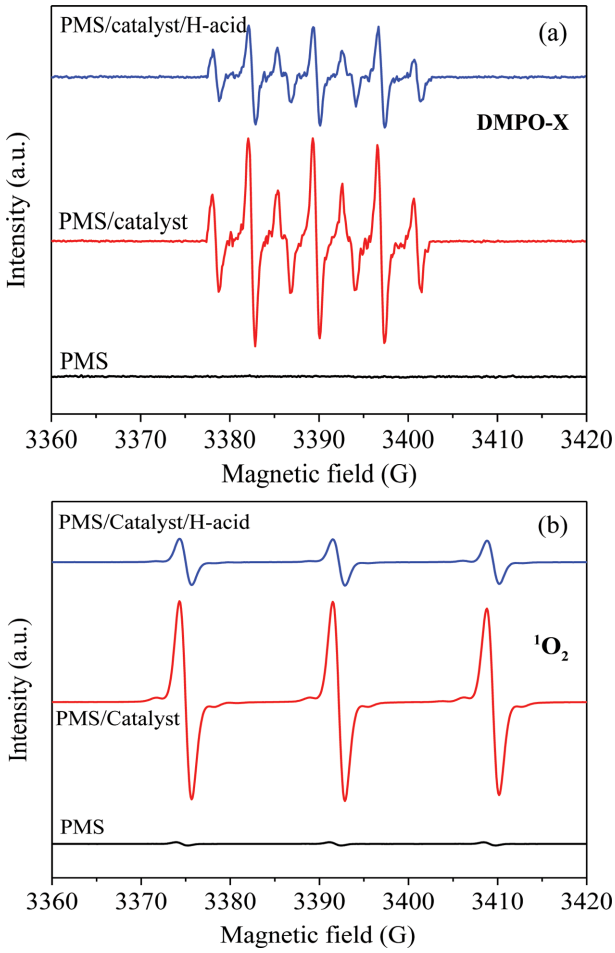


Fig. 7. EPR spectra obtained with DMPO (a) and TEMP (b) as the spin-trapping agents. Reaction conditions: [H-acid]$_0$=20 mg/L, [PMS]$_0$=0.6 mM, [catalyst]=0.5 g/L, [TEMP]$_0$=2 mM, [DMPO]$_0$ =2 mM, pH=5.0, T=25 °C.

son, the degradation of H-acid within 60 min decreased by approximately 56.3% in presence of *L*-histidine, meaning that $^1O_2$ played an important role in the reaction.

EPR tests were further carried to detect the dominant ROSs for H-acid degradation in the Co_3O_4-Fe_2O_3/Al_2O_3/PMS system, using DMPO and TEMP as the spin trapping agents. As shown in Fig. 7(a), no noticeable DMPO-·OH or DMPO-$SO_4^{-\bullet}$ signal could be detected for PMS alone possibly because of the relatively low concentration of the generated radicals in the system. On the contrary, a characteristic signal with an intensity ratio of 1 : 2 : 1 : 2 : 1 : 2 : 1 appeared when Co_3O_4-Fe_2O_3/Al_2O_3 and PMS coexisted in the system. This septuple signal was found in many PMS/catalyst systems and was assigned to the hyperfine splitting of DMPO-X, an oxidized product of DMPO. However, the exact X species that can strongly oxidize DMPO to form DMPO-X are not yet clear; $SO_4^{-\bullet}$ [39,40], $^1O_2$ [41,42], and peroxy radical (ROO·) [43] have been speculated to be the possible ROSs. In addition, some authors attributed this septuple signal to the combination of DMPO-·OH and DMPO-

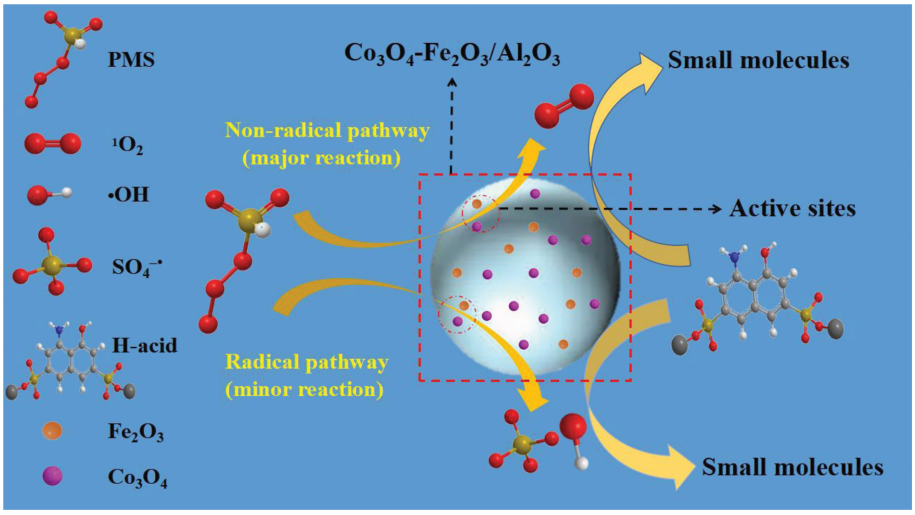


Fig. 8. Proposed activation mechanism of PMS in Co_3O_4-Fe_2O_3/Al_2O_3/PMS system.

$SO_4^{\cdot-}$ adducts [44,45]. Herein, we held a somewhat different viewpoint and suggested that the septuple signal was most possibly caused by the co-attacking of $SO_4^{\cdot-}$/·OH and/or $^1O_2$ on DMPO. The DMPO-X signal substantially weakened after introducing H-acid to the Co_3O_4-Fe_2O_3/Al_2O_3/PMS system, which was the result of the competitive consumption of generated ROSs by H-acid. To confirm the presence of $^1O_2$ in the reaction system as inferred from radical quenching experiments, another group of EPR experiments was also conducted using TEMP as the trapping agent. Fig. 7(b) presents a characteristic three-line signal with equal intensity for the PMS/catalyst system, implying the generation of $^1O_2$. In comparison, the weak signal produced for PMS alone system was also possibly ascribed to $^1O_2$ caused by self-decomposition of PMS [46]. This evidence for the existence of $^1O_2$ can help to explain the marked degradation of H-acid occurring in the presence of PMS alone. After adding H-acid to the Co_3O_4-Fe_2O_3/Al_2O_3/PMS system, the intensity of TEMP-$^1O_2$ signal decreased notably due to the consumption of $^1O_2$ by H-acid. In summary, $^1O_2$ was primarily responsible for the degradation of H-acid, and ·OH and $SO_4^{\cdot-}$ only showed a limited contribution to the degradation. Non-radical pathways were mainly involved in the degradation of H-acid for the Co_3O_4-Fe_2O_3/Al_2O_3/PMS system. The proposed activation mechanism of PMS in Co_3O_4-Fe_2O_3/Al_2O_3/PMS system is illustrated in Fig. 8.

CONCLUSION

A bimetallic Co_3O_4-Fe_2O_3/Al_2O_3 with high metal dispersion was evaluated in terms of PMS activation for H-acid degradation. The degradation efficiency of H-acid was significantly dependent on the metal loading, catalyst dosage, pH, initial concentration of PMS and reaction temperature. The as-prepared Co_3O_4-Fe_2O_3/Al_2O_3 exhibited better reusability than Co/Al_2O_3 due to its relatively low metal leaching and possible redox circle of Co(II)/Co(III). The H-acid degradation over Co_3O_4-Fe_2O_3/Al_2O_3 followed the first-order reaction with activation energies of 42.6 kJ/mol. Both radical and non-radical pathways were involved in the degradation of H-acid in the Co_3O_4-Fe_2O_3/Al_2O_3/PMS system. Of these generated active species, $^1O_2$ played a dominant role in the degradation of H-acid.

ACKNOWLEDGEMENTS

The work was supported by Key Research and Development Plan of Shandong Province (2019GGX104034) and Open Foundation of Key Laboratory of Industrial Ecology and Environmental Engineering, MOE (KLEEE-18-09).

REFERENCES

1. T. Pálfi, E. Takács and L. Wojnárovits, *Water Res.*, **41**, 2533 (2007).
2. T. Olmez-Hanci, I. Arslan-Alaton, D. Orhon, O. Karahan, E. U. Cokgor and G. Insel, *Bioresour. Technol.*, **102**, 5589 (2011).
3. B. Zhao, B. Shi, X. Zhang, X. Cao and Y. Zhang, *Desalination*, **268**, 55 (2011).
4. H. Hayat, Q. Mahmood, A. Pervez, Z. A. Bhatti and S. A. Baig, *Sep. Purif. Technol.*, **154**, 149 (2015).
5. A. Asghar, A. A. A. Raman and W. M. A. W. Daud, *J. Clean. Prod.*, **87**, 826 (2015).
6. B. Yang, Z. Tian, L. Zhang, Y. Guo and S. Yan, *J. Water Process Eng.*, **5**, 101 (2015).
7. R. Feizi, M. Ahmad, S. Jorfi and F. Ghanbari, *Korean J. Chem. Eng.*, **36**, 886 (2019)
8. S. K. Ling, S. Wang and Y. Peng, *J. Hazard. Mater.*, **178**, 385 (2010).
9. Y. Feng, D. Wu, Y. Deng, T. Zhang and K. Shih, *Environ. Sci. Technol.*, **50**, 3119 (2016).
10. J. Deng, S. F. Feng, K. Zhang, J. Li, H. Wang, T. Zhang and X. Ma, *Chem. Eng. J.*, **308**, 505 (2017).
11. E. Saputra, M. A. Budihardjo, S. Bahri and J. A. Pinem, *J. Water Process Eng.*, **12**, 47 (2016).
12. P. Shukla, H. Sun, S. Wang, H. M. Ang and M. O. Tadé, *Catal. Today*, **175**, 380 (2011).
13. Z. Chen, S. Chen, Y. Li, X. Si, J. Huang, S. Massey and G. Chen, *Mater. Res. Bull.*, **57**, 170 (2014).
14. T. Ma, L. Liu, B. Meng, J. Gao, S. Wang and S. Liu, *Sep. Purif. Technol.*, **211**, 298 (2019).
15. W. D. Oh, Z. Dong and T. T. Lim, *Catal. Today*, **280**, 2 (2017).
16. S. Qu, C. Li, X. Sun, J. Wang, H. Luo, S. Wang, J. Ta and D. Li, *Sep. Purif. Technol.*, **224**, 132 (2019).
17. C. di Luca, F. Ivorra, P. Massa and R. Fenoglio, *Ind. Eng. Chem. Res.*, **51**, 8979 (2012).
18. Q. J. Yang, H. Choi, S. R. Al-Abed and D. D. Dionysiou, *Appl. Catal. B: Environ.*, **88**, 462 (2009).
19. L. Samain, A. Jaworski, M. Edén, D. M. Ladd, D. K. Seo, F. J. Garcia-Garcia and U. Häussermann, *J. Solid State Chem.*, **217**, 1 (2014).
20. C. Liu, J. Hong, Y. Zhang, Y. Zhao, L. Wang, L. Wei and J. Li, *Fuel*, **180**, 777 (2016).
21. Y. Mao, W. Li, P. Liu, J. Chen and E. Liang, *Mater. Lett.*, **134**, 276 (2014).
22. X. Zhang, P. Guo, Q. Pan, K. Shi and G. Zhang, *J. Alloy. Compd.*, **727**, 514 (2017).
23. K. E. Dekrafft, C. Wang and W. Lin, *Adv. Mater.*, **24**, 2014 (2012).
24. J. Yang, J. Guo, Y. Wang, T. Wang, J. Gu, L. Peng and W. Ding, *Appl. Surf. Sci.*, **453**, 330 (2018).
25. M. Pal, R. Rakshit, A. K. Singh and K. Mandal, *Energy*, **103**, 481 (2016).
26. L. Zhang, X. Yang, E. Han, L. Zhao and J. Lian, *Appl. Surf. Sci.*, **396**, 945 (2017).
27. D. Flak, Q. Chen, B. S. Mun, Z. Liu, M. Rękas and A. Braun, *Appl. Surf. Sci.*, **455**, 1019 (2018).
28. H. Zhou, K. Li, B. Zhao, W. Deng, Y. Su and F. Zhong, *Chem. Eng. J.*, **326**, 737 (2017).
29. Y. Du, W. Ma, P. Liu, B. Zou and J. Ma, *J. Hazard. Mater.*, **308**, 58 (2016).
30. K. Swaminathan, K. Pachhade and S. Sandhya, *Desalination*, **186**, 155 (2005).
31. N. N. Rao, G. Bose, P. Khare and S. N. Kaul, *J. Environ. Eng.*, **132**, 367 (2006).
32. Y. Yao, C. Xu, J. Qin, F. Wei, M. Rao and S. Wang, *Ind. Eng. Chem. Res.*, **52**, 17341 (2013).
33. Q. Yang, H. Choi and D. D. Dionysiou, *Appl. Catal. B: Environ.*, **74**, 170 (2007).
34. A. Khan, Z. Liao, Y. Liu, A. Jawad, J. Ifthikar and Z. Chen, *J. Hazard. Mater.*, **329**, 262 (2017).

35. X. Zhou, C. Luo, M. Luo, Q. Wang, J. Wang, Z. Liao, Z. Chen and Z. Chen, *Chem. Eng. J.*, **381**, 122587 (2020).
36. R. Yin, W. Guo, H. Wang, J. Du, X. Zhou, Q. Wu and N. Ren, *Chem. Eng. J.*, **334**, 2539 (2018).
37. C. Chen, T. Ma, Y. Shang, B. Gao, B. Jin, H. Dan, Q. Li, Q. Yue, Y. Li, Y. Wang and X. Xu, *Appl. Catal. B: Environ.*, **250**, 382 (2019).
38. P. Liang, C. Zhang, X. Duan, H. Sun, S. Liu, M. O. Tade and S. Wang, *Environ. Sci.: Nano*, **4**, 315 (2017).
39. M. Y. Wei, L. Gao, J. Li, J. Fang, W. Cai, X. Li and A. Xu, *J. Hazard. Mater.*, **316**, 60 (2016).
40. P. Ye, Q. Zou, L. An, Y. Wei, A. Xu and X. Li, *J. Colloid Interf. Sci.*, **535**, 481 (2019).
41. L. Yu, G. Zhang, C. Liu, H. Lan, H. Liu and J. Qu, *ACS Catal.*, **8**, 1090 (2018).
42. P. Bilski, K. Reszka, M. Bilska and C. F. Chignell, *J. Am. Chem. Soc.*, **118**, 1330 (1996).
43. L. Jiang, Y. Zhang, M. Zhou, L. Liang and K. Li, *J. Hazard. Mater.*, **358**, 53 (2018).
44. C. Tan, N. Gao, Y. Deng, J. Deng, S. Zhou, J. Li and X. Xin, *J. Hazard. Mater.*, **276**, 452 (2014).
45. X. Tian, P. Gao, Y. Nie, C. Yang, Z. Zhou, Y. Li and Y. Wang, *Chem. Commun.*, **53**, 6589 (2017).
46. Q. Wang, Y. Shao, N. Gao, W. Chu, J. Chen, X. Lu, Y. Zhu and N. An, *Sep. Purif. Technol.*, **189**, 176 (2017).